ACS Energy LETTERS

http://pubs.acs.org/journal/aelccp

On-Chip Light-Incorporated *In Situ* Transmission Electron Microscopy of Metal Halide Perovskite Materials

Tianwei Duan, Weizhen Wang, Songhua Cai,* and Yuanyuan Zhou*

Cite This: *ACS Energy Lett.* 2023, 8, 3048−3053

Read Online

ACCESS | Metrics & More | Article Recommendations | Supporting Information

ABSTRACT: We report an on-chip light-incorporated *in situ* transmission electron microscopy (LI^{2}ST) approach for probing metal halide perovskites (MHPs) at the nanoscale, realizing the real-time, site-specific tracking of the light-triggered structure transformation. This *in situ* platform is based on a specifically designed microelectromechanical systems (MEMS) chip that offers the capability of light illumination with adjustable intensity and tailorable multiwavelength. The excellent operational reliability of the platform allows for the continuous observation of nanoscale regions of interest, recording the morphological and structural evolutions of perovskite grains and grain boundaries. A proof-of-concept demonstration shows a polycrystalline MHP film undergoing decomposition upon continuous light illumination. Counterintuitively, the decomposition starts and expands within the intragrain regions rather than at the grain boundaries. This work demonstrates an unprecedented ability to reveal light-triggered structural-phase variation for illuminating the dynamic behaviors of MHPs with implications for various energy applications.

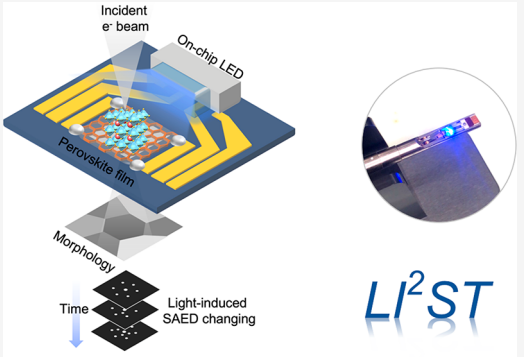

As a new class of light-responsive or light-sensitive materials, metal halide perovskites (MHPs) have demonstrated their promise in numerous optoelectronic device applications.[1−3] The standard MHPs exhibit 3D crystallographic structures with a general formula of ABX_3, where A is cesium, MA^+, or FA^+, B is Pb^{2+}, and X is I^-, Br^-, or Cl^-. The isotropic long-range ordering and the extended inorganic octahedra framework endow 3D perovskites with excellent carrier-transport properties, making them suitable for photovoltaic applications. Thus, the power conversion efficiencies (PCEs) of perovskite-based solar cells (PSCs) have rapidly climbed to 25.7%.[4,5] With the research on MHPs popularized by the photovoltaic (PV) field, this materials' family has been extended to embrace other perovskite and perovskite-like members of various crystallographic dimensionalities (2D, 1D, and 0D), eventually leading to an enormous number of materials with versatile light-responsive characteristics and thus raising much interest beyond the PV community.[6] In particular, the self-trapped excitons resulting from the low electronic dimensionality in these expanded MHP materials contribute to extraordinary emissive behavior under photon excitation and show great potential in light-emitting device applications.[7,8] For all its promise, the active interaction of MHPs with light has been both a blessing and a curse, because while light unleashes materials' functions, it can also trigger materials' transformation and degradation, frequently influencing device performance and stability.[9] In this regard, a fundamental investigation of light-responsive behaviors becomes critical to exploit the full potential of MHPs so that rational engineering strategies can be developed for device improvements.

In situ probes are of vital necessity in this context, as visualizing the sequence of materials' changes provides a landscape for the exploration of the mechanism.[10] Atomic force microscopy (AFM) and synchrotron/laboratory X-ray diffraction are popular methods exploited for studying light responses in MHPs, as these measurements are performed mostly in non-vacuum and open environments where light can be incorporated easily.[11,12] Still, AFM and X-ray probes are limited to revealing either morphological or statistical phase information, calling for the use of analytical transmission electron microscopy (TEM). TEM can simultaneously provide both morphological and phase information, and more

Received: April 10, 2023
Accepted: June 15, 2023
Published: June 20, 2023

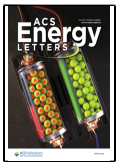

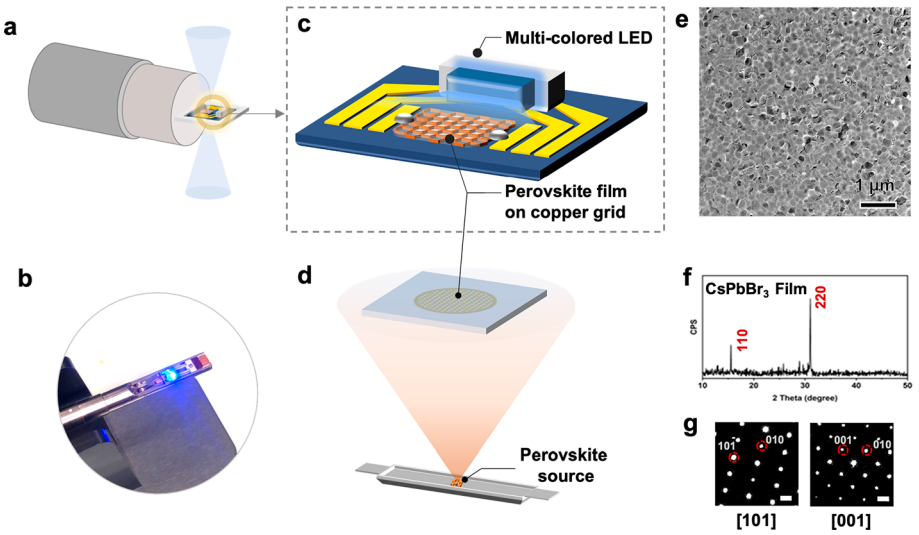

Figure 1. Illustration of on-chip LI^{2}ST for perovskite studies. a, Schematic illustration of the LI^{2}ST holder. b, Photograph showing the LI^{2}ST holder in the light-on state. c, Schematic illustration of the LED-MEMS chip design. d, Schematic illustration of the MHP film deposition onto the grid via thermal evaporation. e, Low-magnification TEM image of the as-deposited MHP. f, XRD pattern of the MHP. g, SAED patterns of two different perovskite grains along the typical zone axis. The scale bar is 1 nm^{-1}.

importantly, unlock an extremely high spatial resolution (from the atomic to nanometer scales).[13−15] The recent development of TEM characterization for MHPs has been proven successful with regard to the unprecedented local structure/phase information and insightful knowledge achieved.[16−20] Nevertheless, it remains an utmost challenge to incorporate a light component into TEM characterization, which has only been tried in only a handful of studies for non-MHP materials systems.[21−24] Generally, commercially available *in situ* TEM platform setups can provide controls only on temperature,[25−27] atmosphere,[28] liquid,[29,30] and electrical bias,[31,32] restricting the study of any light effects on the transformation and degradation of MHPs.[33,34]

In this Letter, we develop an on-chip light-incorporated *in situ* TEM (LI^{2}ST) methodology which can enable us to visualize light-triggered processes in MHPs. The development includes two significant parts, entailing the TEM instrumental innovation and MHP specimen preparation, as schematically illustrated in Figure 1. For the former, we fabricated a silicon-based microelectromechanical systems (MEMS) chip with gold contacts for driving the multi-colored light-emitting diode (LED) light source and one square hole for mounting the TEM sample grid (Figure 1a−c). We first mounted a multi-colored RGB LED on a chip using thermally conductive silicone and then connected the LED electrodes with four outer gold contacts on the chip with conductive Ag paste. The schematic circuit diagram of the multi-colored LED is shown in Figure S1 in the Supporting Information. For the latter, the copper grid covered by the MHP specimen (thermally evaporated, as schematically illustrated in Figure 1d) was loaded onto the square hole located at the center of the chip. Note that spin-coating is an alternative method for depositing the MHP film specimen, while thermal evaporation offers better integrity and thickness uniformity of the sample on the grid.[16] We chose $CsPbBr_3$ for the demonstration of the light effects, because $CsPbBr_3$ is proven to exhibit excellent tolerance to electron doses.[35,36] The as-prepared MHP forms a typical polycrystalline film with near-full coverage and good phase purity (Figure 1e,f). The dominating crystallographic phase is in the orthorhombic *Pbmn* space group, which is further attested by the selected area electron diffraction (SAED) patterns of randomly chosen MHP grains (Figure 1g). To enhance the specimen stability under TEM observation, we further deposited a 10 nm C_{60} layer on top of the MHP film. Then, we cut the carbon grid into an appropriate size and mounted it to exactly cover the square hole on the LED-incorporated MEMS chip. Here we also connected the copper grid with the inner two gold contacts on the MEMS chip with conductive Ag paste (Figure S2a), offering a ground connection of the MHP specimen through the TEM holder to avoid charge accumulation under electron doses.

We highlight three unique features of our LI^{2}ST design. First, the wavelength of light illumination is adjustable by using multi-colored LEDs to meet the experimental requirements (Figure S2b,c). Second, the light intensity is tunable via controlling the flowing current of the LED at forward bias. Third, the LED-MEMS chips are recyclable by simply removing the copper grid and re-mounting a new one, which leads to acost-effective *in situ* TEM solution.

We then performed a validation test on the LI^{2}ST operational reliability. In the light-on state, the silicon substrate and the supporting carbon film on the copper grid could strongly absorb the light, generating a significant amount of heat. According to a previous study,[37] the power absorbed by the silicon substrate is expected to be below 10 W·m^{-2}, for a total of 150 W·m^{-2} light intensity in a similar chip configuration. For the amorphous carbon supporting film, considering the relatively low conductivity (2.2 W·m^{-1}·K^{-1}), a notable thermal expansion is not expected under our specific illumination condition.[38] Although the copper grid framework exhibits a much higher thermal conductivity of 387 W·m^{-1}·K^{-1}, considering the limited size of the sample area (0.25 mm^2), the heat generated from the absorbed light will not cause a substantial linear expansion. As such, Figure 2a,b shows a negligible drift in the TEM imaging when the MHP film sample is studied in the TEM chamber for 60 min in the light-off state. Once the LED is on with an approximate light

https://doi.org/10.1021/acsenergylett.3c00750
ACS Energy Lett. 2023, 8, 3048−3053

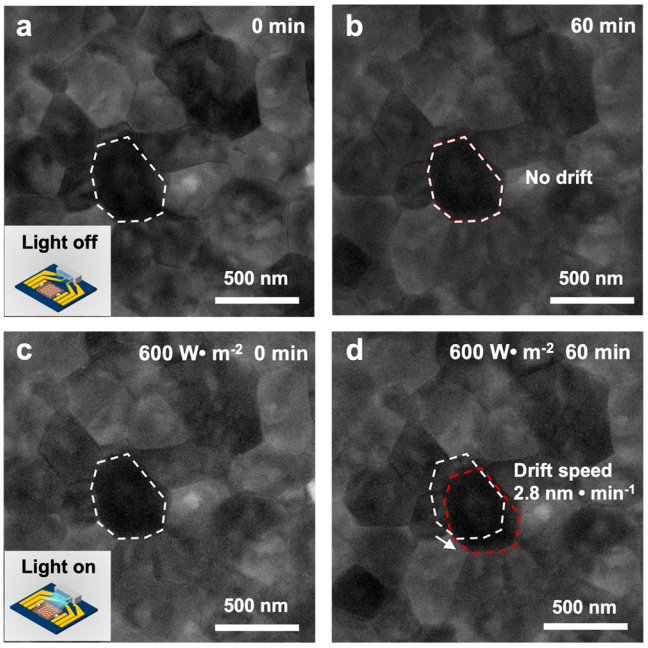

Figure 2. Operational reliability validation of LI²ST. a, b, TEM images acquired in the light-off state at 0 and 60 min, respectively. c, d, TEM images acquired at 0 and 60 min in the light-on state, respectively.

intensity of 600 $W \cdot m^{-2}$, the sample imaging will reach a steady state in ∼5 min. Based on Figure 2c,d, the drifting rate of the MHP sample is still as low as 2.8 $nm \cdot min^{-1}$ within the 60 min of the observation test. This level of stability is expected to be sufficient for acquiring high-resolution scanning transmission electron microscopy (STEM) images and SAED patterns.

We then applied LI²ST to track the morphology and phase evolutions of $CsPbBr_3$ grains (Figure 3). Since $CsPbBr_3$ has an optical bandgap of 2.3 eV, we chose a blue light (450 nm wavelength) to study the light effects. To ensure that any observed changes are induced by light rather than the electron beam, we set an imaging dose rate of 10 $e \cdot nm^{-2} \cdot s^{-1}$, and further, the electron beam was blanked except for the TEM image and SAED pattern acquisition. As seen in Figure 3a, the observed $CsPbBr_3$ film consists of compact grains of ∼500 nm size and well-defined grain boundaries. Figure 3b presents the initial SAED pattern taken from two adjacent MHP grains, as marked by the white circle in the light-off state. The SAED pattern confirms the orthorhombic crystallographic structure of $CsPbBr_3$ observed along the [112] zone axis. There are no notable changes after 60 min (Figure 3c) and 120 min (Figure 3d). The tracked TEM images do not reveal any significant morphological changes over time (Figure S3). This confirms that the low-dose electron beam in our experiment will lead to slight damage to the $CsPbBr_3$ grains within 120 min under our observation conditions. Therefore, we adopted the same experimental setting but switched to the light-on state (Figure 3e). The flowing current of the LED at forward bias was set to 15 mA, with a total input power of ∼55 mW, leading to ∼450 $W \cdot m^{-2}$ illumination intensity. We acquired the initial SAED pattern from another two adjacent $CsPbBr_3$ grains (marked by a white circle in Figure 3e), and the patterns exhibit the consistent orthorhombic phase with a [100] zone axis (Figure 3f). After light illumination for 60 min, an additional diffraction spot emerges in the pattern taken from the same region, as indicated by the blue circle in Figure 3g. After 120 min of illumination, such additional diffraction spots become more populated (Figure 3h), which indicates the formation of new phases triggered by light illumination. We carefully calibrated the evolved new patterns, and the generated phase can probably be assigned to $PbBr_2$ (Figure S5).

Since we could acquire little atomic information on $CsPbBr_3$ grains to resolve the microstructural change using LI²ST in conjunction with a regular TEM (Figure S4), we performed an *ex situ* high-resolution STEM observation using aberration-corrected STEM to unravel structural details correlated to the

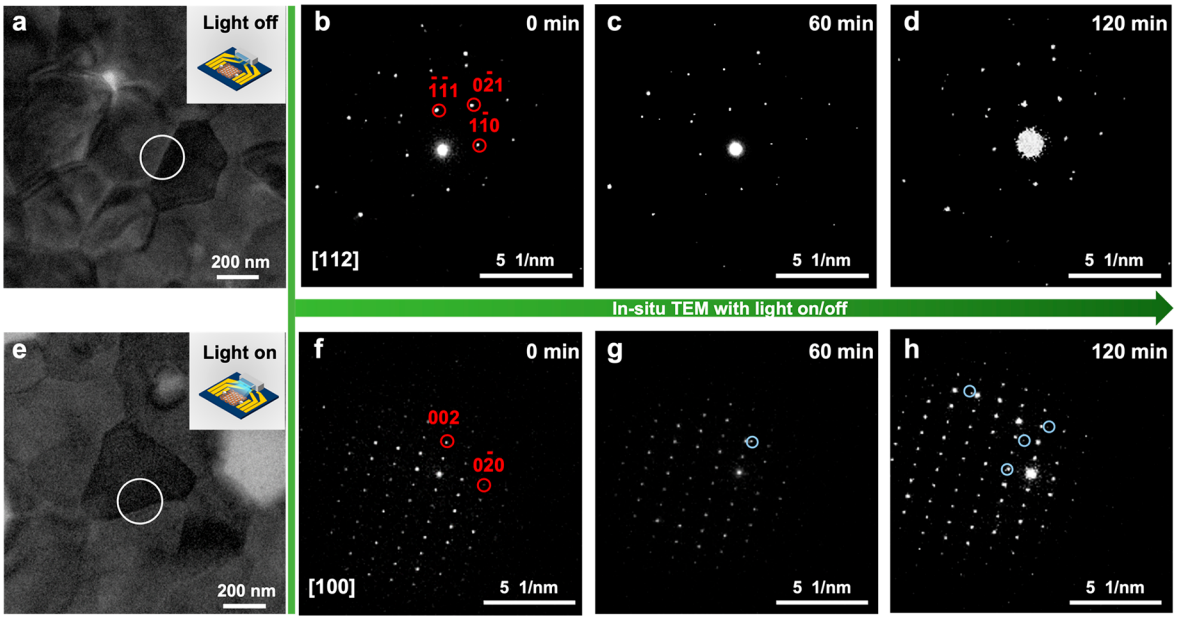

Figure 3. *LI²ST* study of the perovskite film. a, TEM image of perovskite film in the light-off state. b–d, SAED patterns in the light-off state for 0, 60, and 120 min, respectively. e, TEM image of perovskite film in the light-on state. f–h, SAED patterns in the light-on state for 0, 60, and 120 min, respectively.

https://doi.org/10.1021/acsenergylett.3c00750
ACS Energy Lett. 2023, 8, 3048–3053

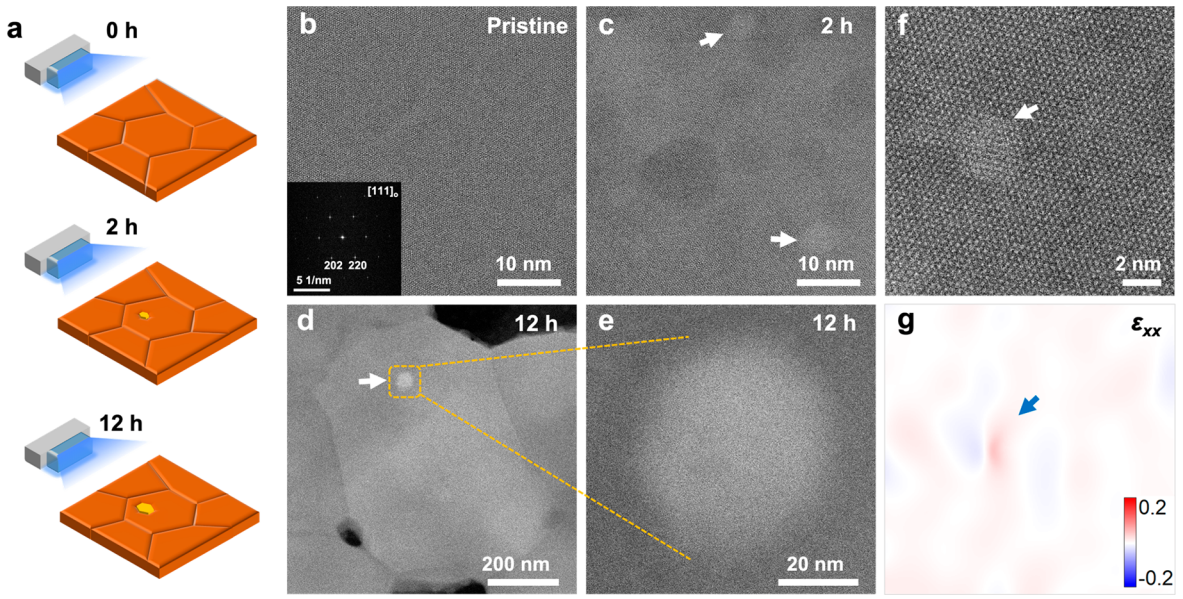

Figure 4. ***Ex situ*** **STEM observation of the light effects on the perovskite film. a, Schematic illustration showing the light-triggered MHP degradation initialization and expansion in the intragrain region. b–d, STEM-HAADF images of the MHP sample after 0, 2, and 12 h illumination in a condition equivalent to the LI^{2}ST case, respectively, showing the intragrain nucleation and growth of $PbBr_2$ impurity clusters (marked using white arrows). e, High-resolution STEM-HAADF image of the $PbBr_2$ impurity cluster in d. f, Atomic-resolution STEM-HAADF image of a single intragrain $PbBr_2$ impurity nanocluster in the sample with 2 h illumination. g, Corresponding in-plane strain ε_{xx} distribution of f generated by GPA analysis.**

SAED evolution. We formed the MHP sample specimen using a method identical to that for the *in situ* experiment, following which we illuminated the sample on the LED-MEMS chip with identical light conditions (Figure 4a). To avoid any electron beam-induced damage, the beam current of the electron probe for high-resolution STEM imaging was reduced to 4 pA. By viewing MHPs with continuous light illumination for different time durations (Figure 4b–e), the dynamic process of the light-triggered perovskite transformation can be resolved. As seen in Figure 4b, the crystal structure of the pristine MHP sample before light illumination is consistent with the orthorhombic $CsPbBr_3$ observed along the [111] zone axis, containing little impurities. After 2 h of illumination, some nanoclusters (in brighter contrast in the scanning transmission electron microscopy–high-angle annular dark field (STEM-HAADF) image) start to emerge (Figure 4c), attributed to the generation of $PbBr_2$. These $PbBr_2$ nanoclusters are mostly distributed in the intragrain regions rather than at grain boundaries (Figure S6). With the illumination extended for 12 h, such nanoclusters grew much larger (Figure 4d,e), suggesting that the perovskite degradation is triggered by the localized expansion of $PbBr_2$ nanoclusters, as illustrated in Figure 4a. By plotting the average size of intragrain $PbBr_2$ nanoclusters as a function of the illumination time (Figure S6), we found that the $PbBr_2$ expansion undergoes an acceleration within the investigated period of light illumination. Furthermore, based on the geometrical phase analysis (GPA) in Figure 4g, the formation of intragrain $PbBr_2$ nanoclusters results in heterogeneous lattice distortion and spatial strain accumulation (Figures 4f,g). This can influence the MHP stability, possibly being responsible for the observed degradation acceleration.

It is counter-intuitive to observe that the light-induced perovskite degradation starts in the intragrain region, although it is difficult to conclude the exact geometric location of these generated phases (either inside or on top of the grain) without tomographic imaging. Generally, the decomposition of polycrystalline MHP thin films is popularly believed to be initialized at grain boundaries in other environmental conditions, such as moisture and oxygen.[39] Therefore, we propose a different microstructural mechanism for light-induced MHP degradation. It was confirmed by Kim et al.[40] that a large tunable photoeffect on ion conduction exists in MHPs. Once an MHP film is exposed to light, it absorbs photons and generates excitons that dissociate into free charge carriers. Along with the augmentation of the electronic carrier concentration, the halide ion conductivity also increases rapidly. As shown in Figure 5, under illumination, Br^- combines with a positively charged hole (h^+) to form neutral bromine (Br^0), i.e., $Br^- + h^+ \rightarrow Br^0$, which can be irreversibly extracted by the high vacuum in TEM. This can create a non-stoichiometry that eventually exceeds the equilibrium homogeneity range of $CsPbBr_3$, causing the observed photo-

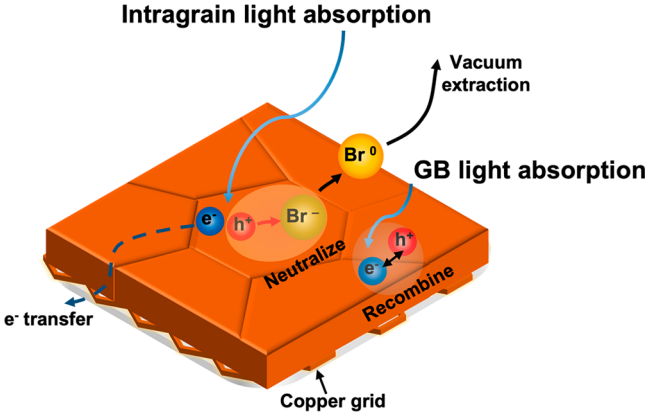

Figure 5. Proposed mechanisms for the observed intragrain-dominated photodecomposition.

https://doi.org/10.1021/acsenergylett.3c00750
ACS Energy Lett. 2023, 8, 3048–3053

decomposition.[40] Such photodecomposition prefers to occur in the intragrain region, because the lifetimes of photogenerated electron−hole carriers are much shorter due to the severe non-radiative recombination in the grain boundary region, reducing the possibility for reaction of Br^- and h^+. Figure 5 schematically illustrates this difference. In addition, the photothermal effects can lead to strain accumulation in the intragrain region, while the flexible atomic arrangement in the grain boundary region can better accommodate lattice distortion and strain evolution. Once the degradation occurs in the intragrain region, as illustrated in Figure 4a, its propagation will be relatively localized, which is different from the case of grain boundary-dominated degradation with a 3D propagation network.[39]

In closing, LI^{2}ST provides a broadly applicable, highly flexible solution for high-resolution *in situ* S/TEM characterizations under adjustable light illumination conditions without any specific modifications to commercial *in situ* TEM hold systems. The unique LED-MEMS chip design is suitable for integrating versatile commercial TEM grids, enabling us to investigate a broad range of light-responsive and light-sensitive samples. Also importantly, we can use LI^{2}ST to investigate perovskite solar cell device specimens fabricated using a focused-ion beam, which will allow us to measure light-driven microstructural dynamics in real devices and correlate it with the widely concerning device stability issue. A thorough understanding of all these fundamental sciences, enabled by LI^{2}ST, will provide us with a comprehensive understanding of structure−property−performance characteristics and will lead to the development of light-responsive materials-based technologies.

■ ASSOCIATED CONTENT

Supporting Information

The Supporting Information is available free of charge at https://pubs.acs.org/doi/10.1021/acsenergylett.3c00750.

Detailed description of experimental methods; Figures S1 and S2 illustrating the design of the LED-MEMS chip and LI^{2}ST holder; Figures S3−S5 showing TEM images and SAED patterns of the perovskite films in both the light-off and light-on states; Figure S6 with S/TEM images showing that the perovskite photodecomposition is frequently initialized in the intragrain regions (PDF)

■ AUTHOR INFORMATION

Corresponding Authors

Songhua Cai − *Department of Applied Physics, The Hong Kong Polytechnic University, Kowloon 999077 Hong Kong SAR, China;* orcid.org/0000-0003-3839-2030; Email: songhua.cai@polyu.edu.hk

Yuanyuan Zhou − *Department of Physics, Hong Kong Baptist University, Kowloon 999077 Hong Kong SAR, China;* orcid.org/0000-0002-8364-4295; Email: yyzhou@hkbu.edu.hk

Authors

Tianwei Duan − *Department of Physics, Hong Kong Baptist University, Kowloon 999077 Hong Kong SAR, China*

Weizhen Wang − *Department of Applied Physics, The Hong Kong Polytechnic University, Kowloon 999077 Hong Kong SAR, China*

Complete contact information is available at: https://pubs.acs.org/10.1021/acsenergylett.3c00750

Notes

The authors declare the following competing financial interest(s): A United States provisional utility patent application (No. 63/507,745) related to this work has been filed.

■ ACKNOWLEDGMENTS

Y.Z. acknowledges the Early Career Scheme (No. 22300221), the General Research Fund (No. 12302822) from the Hong Kong Research Grant Council (RGC), and the Excellent Young Scientists Fund (No. 52222318) from the National Natural Science Foundation of China (NSFC). Y.Z. also acknowledges start-up grants, the Initiation Grant - Faculty Niche Research Areas (IG-FNRA) 2020/21 and the Interdisciplinary Research Matching Scheme (IRMS) 2020/21 from Hong Kong Baptist Univeristy. S.C. acknowledges support from start-up grants from the Department of Applied Physics, the Hong Kong Polytechnic University (1-BD96, 1-BDCM), the Hong Kong RGC General Research Fund (Nos. 15306021 and 15306122), the NSFC Young Scientists Fund (No. 12104381), and the open-topic program of State Key Laboratory of Solid State Microstructures at Nanjing University (No. M34001). T.D. acknowledges the support from the Hong Kong RGC Postdoc Fellowship Scheme. Part of this work was performed on the Hong Kong RGC-supported STEM facilities (No. C5029-18E).

■ REFERENCES

(1) Kojima, A.; Teshima, K.; Shirai, Y.; Miyasaka, T. Organometal Halide Perovskites as Visible-Light Sensitizers for Photovoltaic Cells. *J. Am. Chem. Soc.* **2009**, *131* (17), 6050−6051.

(2) Lim, J.; Kober-Czerny, M.; Lin, Y.-H.; Ball, J. M.; Sakai, N.; Duijnstee, E. A.; Hong, M. J.; Labram, J. G.; Wenger, B.; Snaith, H. J. Long-Range Charge Carrier Mobility in Metal Halide Perovskite Thin-Films and Single Crystals via Transient Photo-Conductivity. *Nat. Commun.* **2022**, *13* (1), 4201.

(3) Gong, J.; Hao, M.; Zhang, Y.; Liu, M.; Zhou, Y. Layered 2D Halide Perovskites beyond the Ruddlesden-Popper Phase: Tailored Interlayer Chemistries for High-Performance Solar Cells. *Angew. Chem. Int. Ed.* **2022**, *134* (10), No. e202112022.

(4) Park, J.; Kim, J.; Yun, H.-S.; Paik, M. J.; Noh, E.; Mun, H. J.; Kim, M. G.; Shin, T. J.; Seok, S. I. Controlled Growth of Perovskite Layers with Volatile Alkylammonium Chlorides. *Nature* **2023**, *616*, 724−730.

(5) Li, L.; Wang, Y.; Wang, X.; Lin, R.; Luo, X.; Liu, Z.; Zhou, K.; Xiong, S.; Bao, Q.; Chen, G.; Tian, Y.; Deng, Y.; Xiao, K.; Wu, J.; Saidaminov, M. I.; Lin, H.; Ma, C.-Q.; Zhao, Z.; Wu, Y.; Zhang, L.; Tan, H. Flexible All-Perovskite Tandem Solar Cells Approaching 25% Efficiency with Molecule-Bridged Hole-Selective Contact. *Nat. Energy* **2022**, *7* (8), 708−717.

(6) Saparov, B.; Mitzi, D. B. Organic-Inorganic Perovskites: Structural Versatility for Functional Materials Design. *Chem. Rev.* **2016**, *116* (7), 4558−4596.

(7) Xu, Z.; Jiang, X.; Cai, H.; Chen, K.; Yao, X.; Feng, Y. Toward a General Understanding of Exciton Self-Trapping in Metal Halide Perovskites. *J. Phys. Chem. Lett.* **2021**, *12* (43), 10472−10478.

(8) Zhang, Y.; Liu, X.; Sun, H.; Zhang, J.; Gao, X.; Yang, C.; Li, Q.; Jiang, H.; Wang, J.; Xu, D. Strong Self-Trapped Exciton Emissions in Two-Dimensional Na-In Halide Perovskites Triggered by Antimony Doping. *Angew. Chem., Int. Ed.* **2021**, *60* (14), 7587−7592.

(9) Doherty, T. A. S.; Nagane, S.; Kubicki, D. J.; Jung, Y.-K.; Johnstone, D. N.; Iqbal, A. N.; Guo, D.; Frohna, K.; Danaie, M.; Tennyson, E. M.; Macpherson, S.; Abfalterer, A.; Anaya, M.; Chiang, Y.-H.; Crout, P.; Ruggeri, F. S.; Collins, S.; Grey, C. P.; Walsh, A.;

Midgley, P. A.; Stranks, S. D. Stabilized Tilted-Octahedra Halide Perovskites Inhibit Local Formation of Performance-Limiting Phases. *Science* **2021**, *374*, 1598−1605.
(10) Meng, X.; Tian, X.; Zhang, S.; Zhou, J.; Zhang, Y.; Liu, Z.; Chen, W. In Situ Characterization for Understanding the Degradation in Perovskite Solar Cells. *Solar RRL* **2022**, *6* (7), 2200280.
(11) Zhou, Y.; Zhou, H.; Deng, J.; Cha, W.; Cai, Z. Decisive Structural and Functional Characterization of Halide Perovskites with Synchrotron. *Matter* **2020**, *2* (2), 360−377.
(12) Gao, Q.; Tsai, W.-Y.; Balke, N. In Situ and Operando Force-Based Atomic Force Microscopy for Probing Local Functionality in Energy Storage Materials. *Electrochemical Sci. Adv.* **2022**, *2* (1), No. e2100038.
(13) Zhou, Y.; Game, O. S.; Pang, S.; Padture, N. P. Microstructures of Organometal Trihalide Perovskites for Solar Cells: Their Evolution from Solutions and Characterization. *J. Phys. Chem. Lett.* **2015**, *6* (23), 4827−4839.
(14) Cai, S.; Zhou, Y. Visualizing the Invisible in Perovskites. *Joule* **2020**, *4* (12), 2545−2548.
(15) Zachman, M. J.; Hachtel, J. A.; Idrobo, J. C.; Chi, M. Emerging Electron Microscopy Techniques for Probing Functional Interfaces in Energy Materials. *Angew. Chem., Int. Ed.* **2020**, *59* (4), 1384−1396.
(16) Rothmann, M. U.; Kim, J. S.; Borchert, J.; Lohmann, K. B.; O'Leary, C. M.; Sheader, A. A.; Clark, L.; Snaith, H. J.; Johnston, M. B.; Nellist, P. D.; Herz, L. M. Atomic-Scale Microstructure of Metal Halide Perovskite. *Science* **2020**, *370* (6516), No. eabb5940.
(17) Cai, S.; Dai, J.; Shao, Z.; Rothmann, M. U.; Jia, Y.; Gao, C.; Hao, M.; Pang, S.; Wang, P.; Lau, S. P.; Zhu, K.; Berry, J. J.; Herz, L. M.; Zeng, X. C.; Zhou, Y. Atomically Resolved Electrically Active Intragrain Interfaces in Perovskite Semiconductors. *J. Am. Chem. Soc.* **2022**, *144* (4), 1910−1920.
(18) Li, Y.; Zhou, W.; Li, Y.; Huang, W.; Zhang, Z.; Chen, G.; Wang, H.; Wu, G.-H.; Rolston, N.; Vila, R.; Chiu, W.; Cui, Y. Unravelling Degradation Mechanisms and Atomic Structure of Organic-Inorganic Halide Perovskites by Cryo-EM. *Joule* **2019**, *3* (11), 2854−2866.
(19) Li, W.; Rothmann, M. U.; Zhu, Y.; Chen, W.; Yang, C.; Yuan, Y.; Choo, Y. Y.; Wen, X.; Cheng, Y.-B.; Bach, U.; Etheridge, J. The Critical Role of Composition-Dependent Intragrain Planar Defects in the Performance of $MA_{1-X}FA_xPbI_3$ Perovskite Solar Cells. *Nat. Energy* **2021**, *6* (6), 624−632.
(20) Chen, S.; Wu, C.; Shang, Q.; Liu, Z.; He, C.; Zhou, W.; Zhao, J.; Zhang, J.; Qi, J.; Zhang, Q.; Wang, X.; Li, J.; Gao, P. Atomic Structure and Electrical/Ionic Activity of Antiphase Boundary in $CH_3NH_3PbI_3$. *Acta Materialia* **2022**, *234*, 118010.
(21) Lu, Y.; Yin, W.-J.; Peng, K.-L.; Wang, K.; Hu, Q.; Selloni, A.; Chen, F.-R.; Liu, L.-M.; Sui, M.-L. Self-Hydrogenated Shell Promoting Photocatalytic H2 Evolution on Anatase TiO_2. *Nat. Commun.* **2018**, *9* (1), 2752.
(22) Hou, C.; Wang, K.; Zhang, W.; Chen, D.; Wang, X.; Fan, L.; Li, C.; Zhao, J.; Dong, L. In-Situ Device-Level TEM Characterization Based on Ultra-Flexible Multilayer MoS_2 Micro-Cantilever. *Adv. Mater.* **2023**, 2301439.
(23) Żak, A. M. Light-Induced In Situ Transmission Electron Microscopy—Development, Challenges, and Perspectives. *Nano Lett.* **2022**, *22* (23), 9219−9226.
(24) Wang, P.; Xu, F.; Gao, P.; Cai, S.; Bai, X. In-Situ Optical TEM. In *In-Situ Transmission Electron Microscopy*; Sun, L., Xu, T., Zhang, Z., Eds.; Springer Nature: Singapore, 2023; pp 151−186.
(25) Divitini, G.; Cacovich, S.; Matteocci, F.; Cinà, L.; Di Carlo, A.; Ducati, C. In Situ Observation of Heat-Induced Degradation of Perovskite Solar Cells. *Nat. Energy* **2016**, *1* (2), 15012.
(26) Fan, Z.; Xiao, H.; Wang, Y.; Zhao, Z.; Lin, Z.; Cheng, H.-C.; Lee, S.-J.; Wang, G.; Feng, Z.; Goddard, W. A.; Huang, Y.; Duan, X. Layer-by-Layer Degradation of Methylammonium Lead Tri-Iodide Perovskite Microplates. *Joule* **2017**, *1* (3), 548−562.
(27) Kim, T. W.; Shibayama, N.; Cojocaru, L.; Uchida, S.; Kondo, T.; Segawa, H. Real-Time In Situ Observation of Microstructural Change in Organometal Halide Perovskite Induced by Thermal Degradation. *Adv. Func. Mater.* **2018**, *28* (42), 1804039.
(28) Han, S.; Cai, C.; Yang, F.; Zhu, Y.; Sun, Q.; Zhu, Y. G.; Li, H.; Wang, H.; Shao-Horn, Y.; Sun, X.; Gu, M. Interrogation of the Reaction Mechanism in a Na-O_2 Battery Using *In Situ* Transmission Electron Microscopy. *ACS Nano* **2020**, *14* (3), 3669−3677.
(29) Ortiz Peña, N.; Ihiawakrim, D.; Han, M.; Lassalle-Kaiser, B.; Carenco, S.; Sanchez, C.; Laberty-Robert, C.; Portehault, D.; Ersen, O. Morphological and Structural Evolution of Co_3O_4 Nanoparticles Revealed by *in Situ* Electrochemical Transmission Electron Microscopy during Electrocatalytic Water Oxidation. *ACS Nano* **2019**, *13* (10), 11372−11381.
(30) Zhang, Q.; Ma, J.; Mei, L.; Liu, J.; Li, Z.; Li, J.; Zeng, Z. In Situ TEM Visualization of LiF Nanosheet Formation on the Cathode-Electrolyte Interphase (CEI) in Liquid-Electrolyte Lithium-Ion Batteries. *Matter* **2022**, *5* (4), 1235−1250.
(31) Jeangros, Q.; Duchamp, M.; Werner, J.; Kruth, M.; Dunin-Borkowski, R. E.; Niesen, B.; Ballif, C.; Hessler-Wyser, A. In Situ TEM Analysis of Organic-Inorganic Metal-Halide Perovskite Solar Cells under Electrical Bias. *Nano Lett.* **2016**, *16* (11), 7013−7018.
(32) Jung, H. J.; Kim, D.; Kim, S.; Park, J.; Dravid, V. P.; Shin, B. Stability of Halide Perovskite Solar Cell Devices: In Situ Observation of Oxygen Diffusion under Biasing. *Adv. Mater.* **2018**, *30* (39), 1802769.
(33) Fan, Z.; Zhang, L.; Baumann, D.; Mei, L.; Yao, Y.; Duan, X.; Shi, Y.; Huang, J.; Huang, Y.; Duan, X. In Situ Transmission Electron Microscopy for Energy Materials and Devices. *Adv. Mater.* **2019**, *31* (33), 1900608.
(34) Kim, M.; Ham, S.-Y.; Cheng, D.; Wynn, T. A.; Jung, H. S.; Meng, Y. S. Advanced Characterization Techniques for Overcoming Challenges of Perovskite Solar Cell Materials. *Adv. Energy Mater.* **2021**, *11* (15), 2001753.
(35) Thind, A. S.; Luo, G.; Hachtel, J. A.; Morrell, M. V.; Cho, S. B.; Borisevich, A. Y.; Idrobo, J.-C.; Xing, Y.; Mishra, R. Atomic Structure and Electrical Activity of Grain Boundaries and Ruddlesden-Popper Faults in Cesium Lead Bromide Perovskite. *Adv. Mater.* **2019**, *31* (4), 1805047.
(36) Zhou, Y.; Sternlicht, H.; Padture, N. P. Transmission Electron Microscopy of Halide Perovskite Materials and Devices. *Joule* **2019**, *3* (3), 641−661.
(37) Cai, S.; Gu, C.; Wei, Y.; Gu, M.; Pan, X.; Wang, P. Development of in Situ Optical-Electrical MEMS Platform for Semiconductor Characterization. *Ultramicroscopy* **2018**, *194*, 57−63.
(38) Bullen, A. J.; O'Hara, K. E.; Cahill, D. G.; Monteiro, O.; von Keudell, A. Thermal Conductivity of Amorphous Carbon Thin Films. *J. Appl. Phys.* **2000**, *88* (11), 6317−6320.
(39) Zhou, Y.; Herz, L. M.; Jen, A. K.-Y.; Saliba, M. Advances and Challenges in Understanding the Microscopic Structure-Property-Performance Relationship in Perovskite Solar Cells. *Nat. Energy* **2022**, *7* (9), 794−807.
(40) Kim, G. Y.; Senocrate, A.; Yang, T.-Y.; Gregori, G.; Grätzel, M.; Maier, J. Large tunable photoeffect on ion conduction in halide perovskites and implications for photodecomposition. *Nat. Mater.* **2018**, *17* (5), 445−449.

https://doi.org/10.1021/acsenergylett.3c00750
ACS Energy Lett. 2023, 8, 3048−3053